Marine Pollution Bulletin 223 (2026) 119027

Contents lists available at ScienceDirect

Marine Pollution Bulletin

journal homepage: www.elsevier.com/locate/marpolbul

Increased suspended particulate matter differentially stimulates ammonium consumption in a eutrophic estuary

Sijing Kang [a], Shuran Yang [a], Min Nina Xu [b], Weiqiang Zhao [c], Jin-Ming Tang [a], Hongyan Bao [a], Xiuli Yan [d], Xiaolin Li [a], Shuh-Ji Kao [b], Jin-Yu Terence Yang [a,*]

[a] State Key Laboratory of Marine Environmental Science, College of Ocean and Earth Sciences, Xiamen University, Xiamen, 361102, China
[b] State Key Laboratory of Marine Resource Utilization in South China Sea, Hainan University, Haikou, 570228, China
[c] Fourth Institute of Oceanography, Ministry of Natural Resources, Beihai, 536015, China
[d] Guangdong Provincial Key Laboratory of Marine Disaster Prediction and Prevention, Institute of Marine Sciences, Shantou University, Shantou, 515063, China

ARTICLE INFO

Keywords:
SPM
Ammonium
Oxidation
Uptake
Estuaries

ABSTRACT

Riverine inputs of ammonium (NH_4^+) and suspended particulate matter (SPM) from human activities have increased significantly over the past few decades, greatly affecting coastal nitrogen cycling and water quality. However, it remains poorly understood how NH_4^+ consumption in eutrophic estuaries responds to increasing SPM levels. Using ^{15}N-labeling techniques, we quantified ammonia oxidation (AO) and ammonium uptake (AU) during SPM addition experiments across the salinity gradient of the Jiulong River Estuary, a typically human-impacted, eutrophic, and turbid estuary in China. The results showed that adding in situ SPM stimulated AO at the freshwater end (salinity 1.1), but had minimal impact on AO or AU in regions with intermediate salinity. At the seawater end (salinity 28.0), in situ SPM increased both AO and AU, especially enhancing AU. Furthermore, adding riverine SPM collected from freshwater, mainly of terrestrial origin, to seawater caused weaker stimulation of NH_4^+ consumption, particularly in AU. These varied responses suggest that NH_4^+ consumption pathways are controlled by substrate availability, particle source, and the composition of ammonia-utilizing microbial communities in the estuary. This study provides new mechanistic insights into how particles influence NH_4^+ dynamics in eutrophic estuaries, with important implications for nitrogen cycling and water quality under increasing human impacts.

1. Introduction

Estuaries, as regions of active land-sea interaction, are undergoing cumulative perturbations from multiple anthropogenic activities (including land-use change, excessive nutrient loads from fertilizers, aquaculture, and sewage) and global change (e.g., ocean acidification and warming) (Scanes et al., 2020; Tanaka et al., 2021; Kennish, 2025). The growing anthropogenic nitrogen (N) exports from rivers have led to eutrophication, resulting in accelerated algal blooms and deteriorating hypoxia in estuaries and coastal waters (Liu et al., 2021; Galloway et al., 2021; Dai et al., 2023; Ormaza-González et al., 2024). Ammonium (NH_4^+) is one of the major human-induced environmental pollutants, and elevated concentrations can substantially degrade water quality in estuaries and coastal regions (Han et al., 2024). The transformation of NH_4^+, particularly its assimilation to organic N and oxidation to nitrite and nitrate, plays a pivotal role in regulating primary production, driving greenhouse gas (CO_2, N_2O) emissions, and consuming oxygen, thereby exerting strong impacts on aquatic ecosystems and the climate (Bowen et al., 2020; Xu et al., 2022; Han et al., 2023). On the other hand, increasing vast quantities of suspended particulate matter (SPM, with the size generally above 0.7 μm; Verdugo et al., 2004) are exported to the coastal ocean (Bianchi et al., 2024; Hou et al., 2024; Liu et al., 2024), which have disturbed the N cycle regionally and globally (Gruber and Galloway, 2008; Wan et al., 2023; Liu et al., 2025). Therefore, understanding the interactions between the concomitantly increased anthropogenic N (especially NH_4^+) inputs and SPM export is essential for assessing their impacts on coastal water quality and marine ecosystems.

NH_4^+ is recognized as a highly reactive N species and is preferentially assimilated by various microorganisms, including bacteria and phytoplankton (Buchanan et al., 2025). In estuarine environments with dissolved oxygen (DO) concentration exceeding ~25 μmol dm^{-3}, ammonia, a neutral form of NH_4^+ in water, can be effectively oxidized to

* Corresponding author.
E-mail address: jyyang@xmu.edu.cn (J.-Y.T. Yang).

https://doi.org/10.1016/j.marpolbul.2025.119027
Received 22 May 2025; Received in revised form 14 November 2025; Accepted 17 November 2025
Available online 20 November 2025

nitrite (NO_2^-) by ammonia-oxidizing bacteria (AOB) and ammonia-oxidizing archaea (AOA) (Tang et al., 2025). This process requires 1.5 mol of O_2 per mole of NH_3 oxidized and concurrently produces 2 mol of H^+ (Stahl and de la Torre, 2012). Consequently, ammonia oxidation can exacerbate hypoxia and contribute to acidification in many eutrophic estuaries and coastal waters, including the Chesapeake Bay, the Yangtze River estuary, and the Upper Gulf of Thailand (Dai et al., 2023, and references therein). Moreover, this chemoautotrophic pathway supplies substrates for N-removal processes such as denitrification, which is commonly coupled with the release of N_2O (Tan et al., 2020; Yang et al., 2022). Notably, ammonia-derived N_2O has been identified as the dominant source of riverine N_2O emissions, representing a substantial contribution to the global N_2O budget (Stein and Yung, 2003; Wang et al., 2024). SPM hosts diverse assemblages of ammonia oxidizers, typically dominated by the AOB genus *Nitrosomonas* and the archaeal genus *Nitrososphaera*, which actively utilize NH_4^+ released through the remineralization of particle-associated organic substrates (Kuypers et al., 2018; Cai et al., 2019; Kache et al., 2021). Elevated ammonia oxidation rates have been reported in turbid estuaries, including those of the Baltic Sea and several Asian rivers (Xia et al., 2009; Hsiao et al., 2014; Bartl et al., 2019; Ma et al., 2021). Accordingly, particle enrichment in estuarine environments is expected to shape the composition and activity of NH_4^+-based microbial communities, thereby influencing the dynamics of NH_4^+ consumption.

The NH_4^+ consumption rates and their influencing factors (e.g., substrate, temperature, light, total suspended matter, salinity, biological community compositions) have been archived in many estuaries (Zheng et al., 2017; Yan et al., 2019; Zheng et al., 2020; Kache et al., 2021; Tang et al., 2022; Xu et al., 2022). However, knowledge of how increasing concentrations of SPM from different sources would affect the dual NH_4^+ consumption pathways (i.e., assimilation and ammonia oxidation) in human-perturbed estuaries remains limited. To assess this issue, we manipulated in situ and riverine particle addition experiments to quantify responses of ammonia oxidation rates (AOR) and ammonium uptake rates (AUR) in the Jiulong River Estuary (JRE), located in southeastern China (Fig. 1).

The JRE drains a watershed of 14,741 km^2 and discharges on average 1.4×10^{10} m^3 yr^{-1} (Zhang et al., 2022). The basin supports a dense population (~7 million residents in 2021) and has experienced rapid economic growth over the past few decades. Fertilizer use and livestock production have increased 6–10 fold, while gross industrial output has expanded nearly 100 fold (Yan et al., 2012; Dai et al., 2023). The flux of dissolved inorganic nitrogen (DIN) from the JRE is estimated at approximately 34.8 Gg N yr^{-1}, which is higher than or comparable to those reported for other tropical and subtropical estuaries (Yan et al., 2012; Sharples et al., 2017; Ormaza-González et al., 2024). Additionally, the JRE exports DIN at an exceptionally high areal yield rate of 2.3×10^3 kg N km^{-2} yr^{-1}, greatly exceeding those of many of the world's largest rivers, including the Yangtze (0.6×10^3 kg N km^{-2} yr^{-1}) and the Amazon (0.07×10^3 kg N km^{-2} yr^{-1}) Rivers (Yan et al., 2012). These anthropogenic DIN inputs have contributed to recurrent eutrophication in the coastal waters of the JRE (Han et al., 2024). Among DIN species, NH_4^+ fluxes have increased more than 20-fold since the 1980s, attaining 0.6×10^3 kg N km^{-2} yr^{-1} by 2015 (Wu et al., 2017). DIN concentrations in the upper JRE reach up to 250 μmol dm^{-3}, approximately 2–3 times higher than in the 1980s, a pattern consistent with trends observed in the Yangtze and Mississippi Rivers (Yan et al., 2012). In addition to high DIN loads, the JRE also exports substantial organic matter, with fluxes as high as 50×10^6 kg C yr^{-1} in the early 2010s, comparable to those of much larger rivers; Around 75 % of this organic matter is delivered to the adjacent coastal ocean (Wang et al., 2022). The estuary is further characterized by elevated total suspended matter (TSM), averaging ~200 mg dm^{-3} in the upper estuary and ranging between 20 and 40 mg dm^{-3} downstream (Wan et al., 2023). These high TSM concentrations may markedly regulate the NH_4^+ consumption pathways and estuarine biogeochemistry (Lin et al., 2020; Wan et al., 2023). Ammonia consumption rates in the JRE, including ammonia oxidation (5–850 nmol dm^{-3} h^{-1}) and ammonium uptake (6–138 nmol dm^{-3} h^{-1}), have been previously reported, showing a general downstream decline (Yan et al., 2019; Tang et al., 2022). These magnitudes and spatial patterns are comparable to those observed in other eutrophic river systems, such as the Chesapeake Bay, the Mississippi River plume, and European estuaries along the Atlantic coast (Middelburg and Nieuwenhuize, 2000; Wawrik et al., 2004; Laperriere et al., 2019; Kitzinger et al., 2019). Given these characteristics, the JRE provides an ideal natural laboratory for investigating particle-associated NH_4^+ consumption processes.

In this study, two particle-addition treatments were designed to simulate contrasting scenarios: (1) increased particle concentration under in situ estuarine conditions, and (2) rapid transport of riverine particles into coastal seawater. These experiments aim to improve our understanding of particle-mediated alterations in N cycling dynamics in estuaries, and provide insights into biogeochemical models and policy-making to effectively assess NH_4^+-related environmental risks (e.g., ocean deoxygenation and N_2O emissions).

2. Materials and methods

2.1. Sample collection and chemical analysis

To capture a wide salinity gradient, surface water samples were

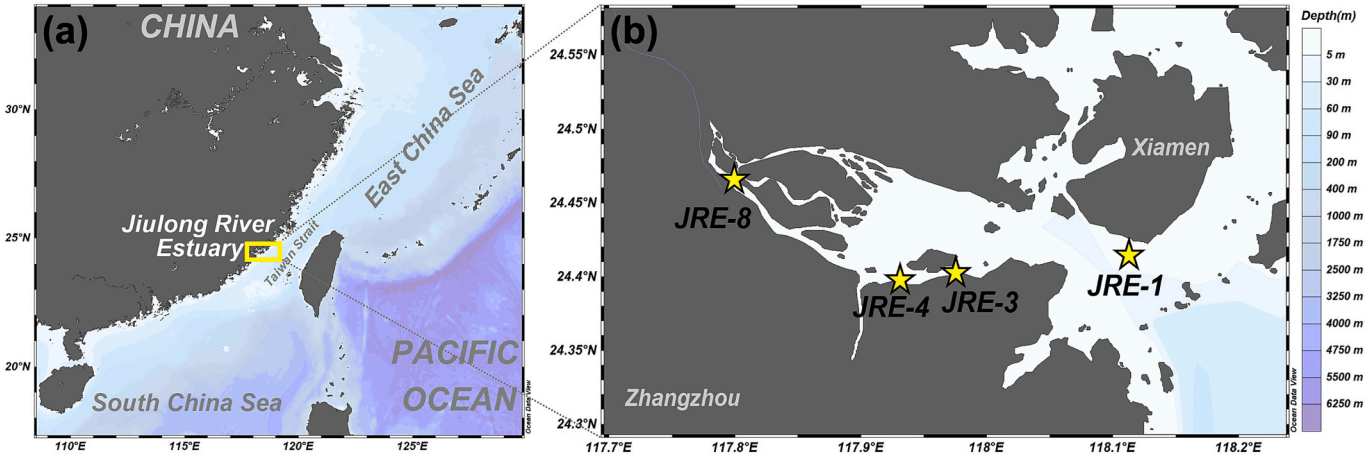

Fig. 1. (a) Location of the Jiulong River Estuary (JRE) and (b) the sampling stations (yellow stars) along the JRE. (For interpretation of the references to color in this figure legend, the reader is referred to the web version of this article.)

collected from four stations spanning the freshwater end to the coastal region of the JRE aboard R/V *Ocean II* on April 19, 2022 (Fig. 1). The cruise coincided with a period of elevated river discharge and a spring tide, under cloudy conditions with occasional light rain and average wind speeds below 4 m s^{-1}. At each station during high tide, 12–18 dm^3 of water was collected from ~0.5 m depth, as determined by rope deployment, using an acid-washed custom-built plexiglass (polymethyl methacrylate) sampler (5 dm^3 volume) (Yan et al., 2019). Samples were subsequently transferred into 20 dm^3 acid-washed polycarbonate bottles. An aliquot of 50 cm^3 of water was filtered through a 0.22 μm syringe polyethersulfone filter. The filtrate was preserved in 50 cm^3 polypropylene centrifuge tubes (BD FALCON). 100–300 mL of water samples were filtered through pre-combusted (at 450 °C for 4 h) and pre-weighed glass fiber filters (0.7 μm pore size and 47 mm diameter, GF/F, Whatman, GE Healthcare, USA) to collect particles. All the samples were frozen at −20 °C until the analysis.

Seawater salinity and temperature were measured using a conductivity-temperature-depth profiler and a portable multiparameter water quality analyzer (WTW, Multi 3630 IDS Set F). NH_4^+, NO_2^-, and NO_x^- ($NO_2^- + NO_3^-$) in the filtrate were determined by classical colorimetric methods with a four-channel Continuous Flow Technicon AA3 Auto-Analyzer (Ban-Lube, GmbH) (Armstrong et al., 1967; Strickland and Parsons, 1972; Becker et al., 2020). The detection limits were 0.1 μmol dm^{-3} for NO_3^-, 0.04 μmol dm^{-3} for NO_2^-, and 0.5 μmol dm^{-3} for NH_4^+. Although the samples were stored frozen for less than a month prior to analysis, we acknowledge that such storage can introduce biases, particularly for NH_4^+. Previous studies have reported measurable losses of NH_4^+ during short-term freezing (Gardolinski et al., 2001). We therefore interpret our nutrient data with caution, recognizing this as a limitation of the study.

All filters were freeze-dried (CoolSafe Freeze Dryer, ScanVac) for 24 h, and then acidified with 1 cm^3 of 1 mol dm^{-3} HCl to remove inorganic carbon from the particles. After that, the decarbonated particulate samples were dried at 60 °C for at least 24 h. We analyzed particulate organic carbon (POC) and nitrogen (PN) contents, and carbon isotopic composition of particulate organic matter, POM ($\delta^{13}C_{org} = (({}^{13}C/{}^{12}C_{sample}) / ({}^{13}C/{}^{12}C_{standard}) - 1) \times 1000‰$, which is referenced to Pee Dee Belemnite, PDB) using an elemental analyzer connected to an isotope ratio mass spectrometer (EA-IRMS, Isoprime 100, UK). The analytical precisions of POC, PN, and $\delta^{13}C_{org}$ were better than 0.1 %, 0.1 % and 0.1 ‰, respectively, based on long-term measurements of the international standard USGS40 (L-glutamic acid; $\delta^{13}C_{org} = -26.39$ ‰) (Yang et al., 2017).

2.2. Particle addition experiments

2.2.1. In situ SPM addition experiments

Water samples collected at ~0.5 m of each station were first quantitatively dispensed into 1 dm^3 acid-washed polycarbonate (PC) bottles ($n = 6$–8) and stored in the dark. Approximately 100–400 cm^3 of water samples at the same depth were subsequently filtered separately using 47 mm track-etched membranes (0.2 μm pore size, Whatman, Nuclepore). After filtration, the membranes were wrapped in pre-combusted (450 °C for 4 h) aluminum foil and frozen at −20 °C to inactivate particles. Water and particle samples were transported to the laboratory within 6 h before the incubation experiments. In the laboratory, the surface waters collected at each station were mixed with the in situ particles on the membranes, representing the in situ SPM addition group ($n = 4$). The control group ($n = 2$) was set as the water samples without particle addition (Fig. S1). The PN concentrations in the in situ SPM addition groups were approximately 7–31 % higher than those in the control groups, due to the particle heterogeneity (Fig. S2). Note that based on the actual amounts of PN added, the in situ SPM addition experimental groups (n = 4) mentioned above can be classified into less (n = 2) and more (n = 2) SPM addition groups.

The ^{15}N-labeled method was used to determine the water-column AUR and AOR (e.g., Xu et al., 2022). $^{15}NH_4Cl$ (99 atom% ^{15}N; Cambridge Isotope Laboratories, Inc., Lot#I-24891C) tracers were introduced into the 1 dm^3 PC bottles for both the in situ particle addition and control groups, yielding final ^{15}N concentrations close to ~20 % of the ambient substrate concentrations (Table S1). While water transparency was not directly measured with a Secchi disk during the cruise, both in situ surveys and remote sensing analyses indicate that Secchi disk depths typically range from 0.2 to 1.4 m along our transect (Lee et al., 2016, 2017). Previous observations demonstrate that the JRE is highly turbid, particularly near the river mouth (Yan et al., 2019; Wan et al., 2023), resulting in very low transparency, with 0.1–1 % surface photosynthetically active radiation (PAR) depths of 0.6–3.0 m even during the daytime (Fig. S3; Tang et al., 2022). During the cruise, observed TSM concentrations (Zhao et al., 2025) were higher than those reported by Tang et al. (2022), further supporting rapid light attenuation in the surface waters of the JRE. Such darkness or low-light conditions in turbid estuaries are expected to intensify as particle abundance increases. Moreover, nitrification rate measurements are conventionally incubated in the dark because light inhibits nitrification (Merbt et al., 2012). Collectively, these considerations justify our assumption that dark incubations realistically represent in situ light conditions at the sampling depth (~0.5 m). Accordingly, all incubation bottles were wrapped in aluminum foil to ensure darkness and maintained at in situ temperature (~23.6 °C; Table S1). To examine the linearity of ^{15}N production in the product pool during incubation, we conducted 12-h incubations with multiple sampling intervals (0, 3, 6, and 12 h; Fig. S4). Once the tracer injection was finished, approximately 120 cm^3 of water sample was filtered immediately through 25 mm diameter 0.37 μm glass fiber membranes (pre-combusted at 450 °C for 4 h) to represent the initial condition (t_0). The remaining water subsamples were terminated at t_1, t_2, and t_3 using the same protocol as the t_0 samples. The filtrate and filters were stored at −20 °C for isotope analysis.

2.2.2. Riverine SPM addition experiments

During the cruise, riverine SPM was collected from the freshwater end at the inner estuary station JRE-8 (salinity 1.1). Water samples were obtained from the seawater end at the outer estuary station JRE-1 (salinity 28.0). Riverine SPM and seawater samples were collected and preserved as described above. Likewise, riverine particles were incorporated into seawater to represent the riverine SPM addition group ($n = 4$), while the control group ($n = 2$) was set as the seawater samples without adding riverine SPM. The same ^{15}N-labeled method and protocol shown above were used to measure the water-column AUR and AOR in this experiment (Fig. S1).

2.2.3. Rate calculation

Nitrogen isotopic composition ($\delta^{15}N = (({}^{15}N/{}^{14}N_{sample}) / ({}^{15}N/{}^{14}N_{standard}) - 1) \times 1000‰$, which is referenced to air N_2) of NO_x^- was determined by the "denitrifier" method (Sigman et al., 2001; Casciotti et al., 2002). Briefly, NO_x^- was quantitatively converted into N_2O gas by the bacterial strain *Pseudomonas aureofaciens* (ATCC#13985), and its $\delta^{15}N$ was subsequently measured using a Thermo Finnigan Gasbench II system interfaced with a Delta V PLUS isotope ratio mass spectrometer. The $\delta^{15}N$ of NO_x^- was calibrated against three international isotope references ($\delta^{15}N_{IAEA\text{-}N3} = 4.70$ ‰, $\delta^{15}N_{USGS34} = -1.80$ ‰, $\delta^{15}N_{USGS32} = 180.00$ ‰). The standard deviation of $\delta^{15}N$ was less than 0.2 ‰ (Yang et al., 2022). The $\delta^{15}N$ of PN was measured using an EA-IRMS described above, with a precision better than 0.2 ‰ (Yang et al., 2017).

The AOR and AUR were determined based on the increases in ^{15}N in the product pool (i.e., NO_x^- and PN) during the incubation period (Dugdale and Wilkerson, 1986; Xu et al., 2022). Based on the correlated linearity in ^{15}N of the product (Fig. S4) during time-series incubation experiments, we calculated the rates as the average ^{15}N accumulation between the t and t_0 points (including t_0-t_1, t_0-t_2, and t_0-t_3).

The AOR was calculated as Eq. (1):

$$\mathrm{AOR} = \frac{\Delta\left[{}^{15}\mathrm{NO}_{\mathrm{X}}^{-}\right]}{\mathrm{t}} \times \left[\frac{\left({}^{14}\mathrm{NH}_4^{+} + {}^{15}\mathrm{NH}_4^{+}\right)}{{}^{15}\mathrm{NH}_4^{+}}\right] \quad (1)$$

where $\Delta[{}^{15}NO_X^-]$ is the change in ^{15}N concentration of the NO_x^- pool between the beginning point t_0 and the end point t of the incubation; t is the incubation interval in hours; $^{14}NH_4^+$ and $^{15}NH_4^+$ are the measured NH_4^+ content in the incubation bottle and the $^{15}NH_4^+$ concentration at the start of the incubation after adding $^{15}NH_4Cl$, respectively.

The AUR was determined using Eq. (2):

$$\mathrm{AUR} = \frac{\Delta\left[{}^{15}\mathrm{PN}\right]}{\mathrm{t}} \times \left[\frac{\left({}^{14}\mathrm{NH}_4^{+} + {}^{15}\mathrm{NH}_4^{+}\right)}{{}^{15}\mathrm{NH}_4^{+}}\right] \quad (2)$$

where $\Delta[^{15}PN]$ is the change in ^{15}N concentration of the PN pool between the beginning and the end points during the incubation experiment. The other parameters are the same as those in Eq. (1).

2.3. Statistical analysis

The statistical significance of NH_4^+ transformation rates in particle addition and control groups was determined using Student's *t*-tests. Pearson's correlation was applied to evaluate the relationships between environmental parameters and NH_4^+ transformation rates. Unless otherwise stated, all the statistical analyses were conducted by GraphPad Prism 9 at a 0.05 significance level.

3. Results and discussion

3.1. Environmental parameters

Environmental conditions across the JRE transect reflected a typical estuarine gradient. During the cruise, the salinity increased from 1.1 in the inner estuary to 28.0 in the outer estuary, while surface temperature remained nearly constant (23.6–23.7 °C; Table S1). For convenience, we defined the sampling sites as representing freshwater, brackish water, saline water, and seawater ends, respectively. Concentrations of NO_3^-, NO_2^-, and NH_4^+ generally declined seaward, showing approximately conservative mixing patterns, with a slight removal at JRE-3 (Fig. 2a–c). NO_3^- was the dominant DIN species, ranging from 34.0 to 178.3 μmol N dm^{-3}, whereas NO_2^- concentrations were an order of magnitude lower (1.60 to 12.11 μmol N dm^{-3}). NH_4^+ concentrations decreased from 34.5 μmol N dm^{-3} at the freshwater end (JRE-8) to 12.5 μmol N dm^{-3} at the seawater end (JRE-1) with the minimum value at JRE-3 (Fig. 2c). These relatively conservative patterns of nutrients along the JRE can be attributed to the frequent water exchange, resulting in a short water residence time (Yan et al., 2019).

The PN distribution resembled the nutrient patterns, showing a decreasing trend with salinity, with the maximum value of 20.7 μmol N dm^{-3} in freshwater and the minimum value of 2.4 μmol N dm^{-3} in seawater (Fig. 2d). In contrast, C/N ratios and $\delta^{13}C_{org}$ values displayed non-conservative patterns (Fig. 2e–f). Specifically, the low- and mid-

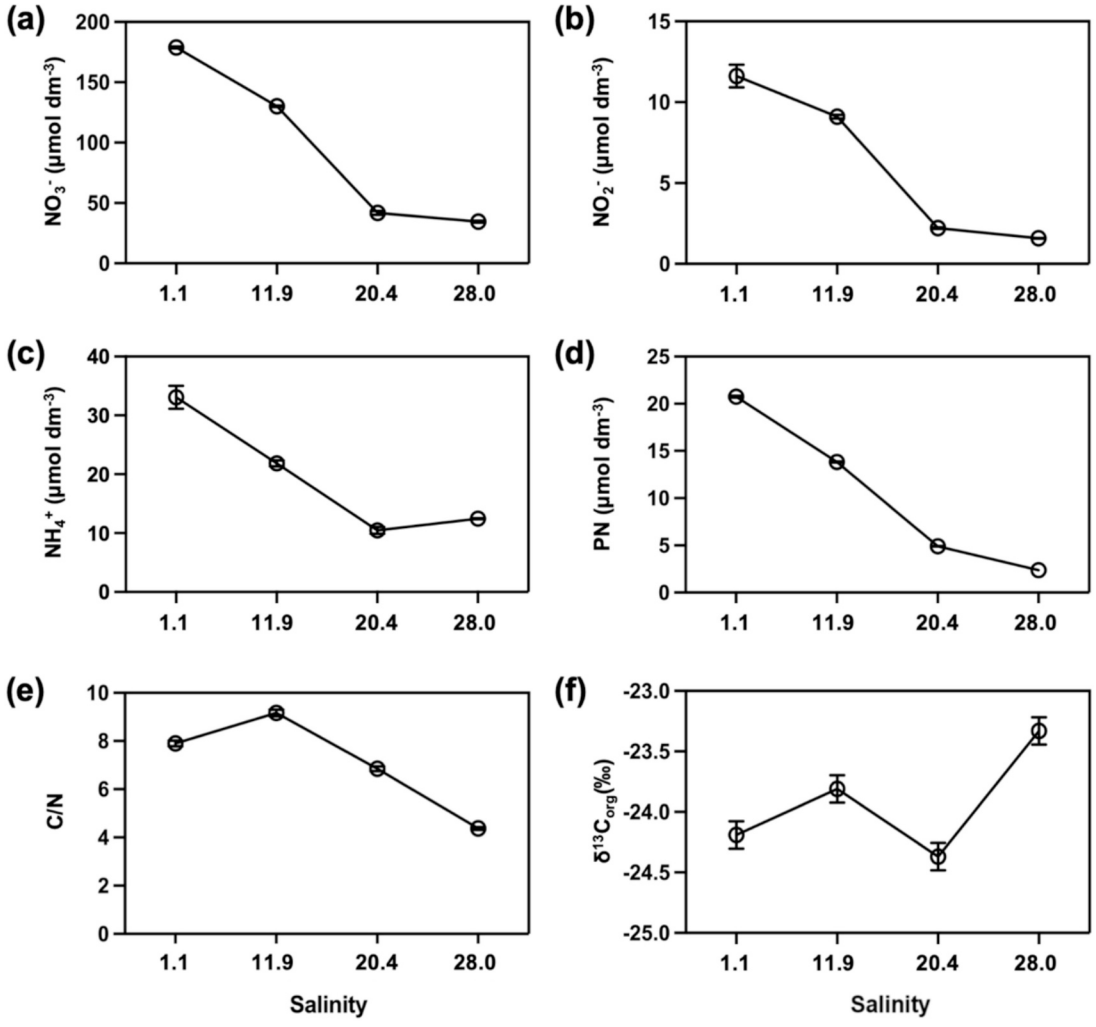

Fig. 2. Distribution of environmental parameters against salinity: (a) nitrate (μmol dm^{-3}); (b) nitrite (μmol dm^{-3}); (c) ammonium (μmol dm^{-3}); (d) particulate nitrogen (PN, μmol dm^{-3}); (e) C/N ratios of POM; (f) $\delta^{13}C_{org}$ of POM (‰).

salinity stations (JRE-8, JRE-4, and JRE-3) exhibited higher C/N ratios (6.9–9.2) and lower $\delta^{13}C_{org}$ values (−24.4 ‰ to −23.8 ‰), whereas the high-salinity station (JRE-1) showed a lower C/N ratio (4.4) and a higher $\delta^{13}C_{org}$ value (−23.3 ‰). These contrasting trends indicate a clear transition in organic matter sources, from terrestrial-dominated particulate organic matter (POM) in the inner estuary to marine-derived POM in the outer estuary, as observed in other estuaries (Lamb et al., 2005; Ye et al., 2017). Together, these environmental characteristics provide the framework for understanding the observed NH_4^+ consumption pathways along the salinity gradient.

3.2. NH_4^+ consumption pathways and their influencing factors

Against the environmental backdrop, both AOR and AUR at four stations along the salinity gradient were quantified based on the time-series ^{15}N tracer incubation experiments. The ambient AOR (i.e., control groups; Fig. 3) showed the highest value of 68.8 nmol N dm^{-3} h^{-1} at the freshwater end (JRE-8) with a slight decrease at JRE-4, and then rapidly dropped to 1.0 nmol N dm^{-3} h^{-1} at the downstream stations (JRE-3 and JRE-1). The ambient AUR also decreased with salinity but varied over a narrow range (33.8–97.1 nmol N dm^{-3} h^{-1}; Fig. 3b). These rates are comparable to those reported previously for the JRE (Yan et al., 2019; Yu et al., 2019; Tang et al., 2022), and are consistent with patterns observed in other estuaries with steep physiochemical gradients (e.g., salinity, PN, and nutrients) (Berounsky and Nixon, 1993; Tang et al., 2022; Xu et al., 2022).

At the freshwater and brackish stations (JRE-8 and JRE-4), the ambient AUR and AOR were of similar magnitude, suggesting that planktonic microorganisms capable of assimilating NH_4^+ compete for substrates at a level similar to that of ammonia-oxidizing microorganisms (Figs. 3 and S5). However, downstream stations exhibited disproportionately low AOR, despite NH_4^+ concentrations not being depleted, even under dark conditions, indicating that NH_4^+ assimilation by planktonic communities may outcompete NH_4^+ oxidation under higher salinity conditions (Fig. S5). This interpretation is supported by microbial community analyses, which show that bacterial *amoA* genes were more abundant at the freshwater end, while archaeal *amoA* genes increased with increasing salinity (Fig. S6). However, because AOA are characterized by high substrate affinity and typically dominate under NH_4^+-depleted conditions (Ma et al., 2021; Dai et al., 2022), their activities may have been suppressed in the outer estuary where NH_4^+ concentrations remained relatively high (exceeded 10 μmol dm^{-3}; Figs. 2c and 3a). Consequently, phytoplankton-mediated NH_4^+ uptake likely dominated NH_4^+ consumption in the outer JRE, as potential competition from AOB and AOA and/or environmental stressors was alleviated.

3.3. Responses of ammonium consumption pathways to in situ SPM addition

To comprehensively elucidate the role of elevated particle concentrations in modulating NH_4^+ consumption within the eutrophic estuary, we systematically quantified the responses of AOR and AUR to the addition of in situ SPM along the salinity gradient of the JRE. The results revealed divergent responses (Fig. 3a–b). Specifically, at the freshwater end (JRE-8), SPM addition enhanced AOR by ~76 % but had little effect on AUR. In contrast, at the seawater end (JRE-1), AOR and AUR increased by ~15 % and ~69 %, respectively. No statistically significant changes in these NH_4^+ consumption pathways were detected at the mid-salinity zones.

Our experimental findings show that increased ambient SPM concentrations can alter the natural rates of NH_4^+ consumption pathways

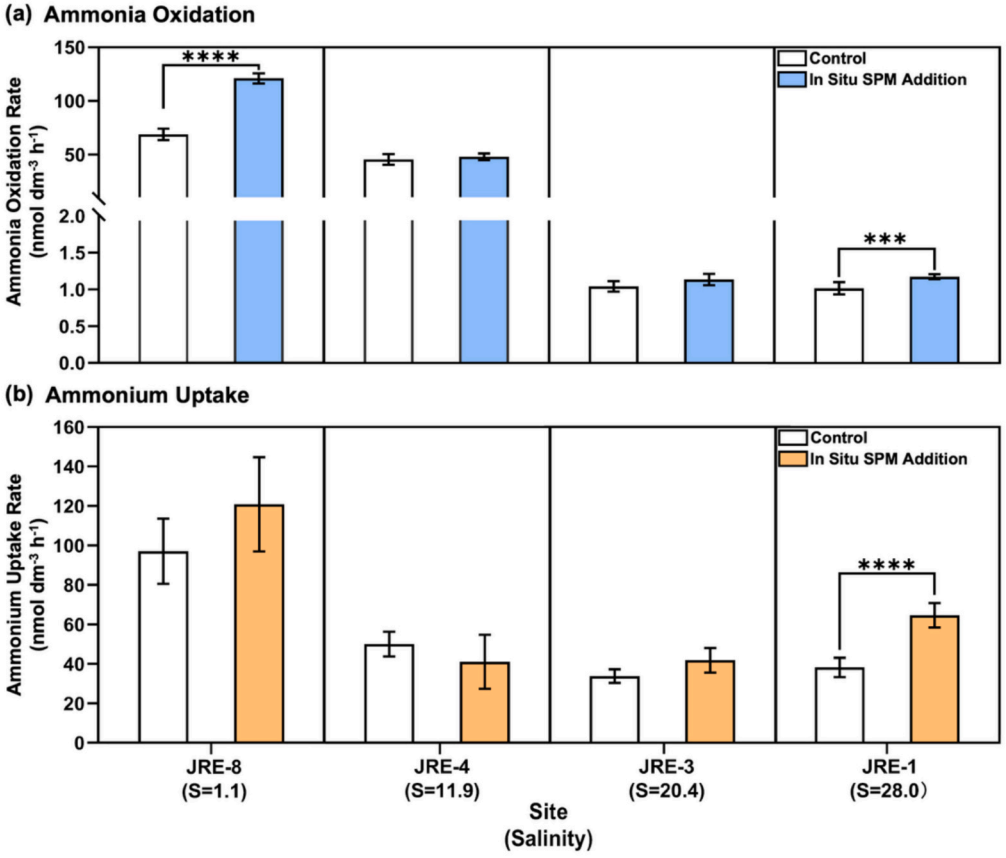

Fig. 3. Comparisons of (a) AOR and (b) AUR without (Control; white bars) and with in situ particle addition (colored bars) at four stations across the salinity gradient in the JRE (**: $p < 0.01$, ***: $p < 0.001$, ****: $p < 0.0001$).

along the salinity gradient of the JRE. In the inner estuary, NH_4^+ is quickly oxidized to NO_2^- and NO_3^-, whereas in the outer estuary, it is predominantly assimilated into particulate forms. We also quantitatively assess how the NH_4^+ turnover time per unit increase in PN changes along the JRE (Fig. S7). A 1 μmol dm^{-3} increase in ambient PN shortened the NH_4^+ turnover time by 1.61 ± 0.26 days in the inner estuary, but by 33.40 ± 5.92 days in the outer estuary. Thus, particle-mediated acceleration of NH_4^+ consumption was most pronounced at the freshwater and seawater ends, resulting in a shorter NH_4^+ turnover time than reported earlier (Wang et al., 2015; Tang et al., 2022).

In the following, we will discuss the potential mechanisms underlying the distinct responses of AOR and AUR to SPM addition along the environmental gradient of the JRE. Due to particle heterogeneity, the actual added PN in the quadruplicate samples at each site was not entirely the same. However, the results between the less ($n = 2$) and more ($n = 2$) SPM addition groups were statistically consistent (Fig. S8), indicating that differences in added PN concentrations did not change overall response patterns of AOR and AUR along the salinity gradient. In addition, time-series monitoring revealed the rapid remineralization of the added SPM, as evidenced by NH_4^+ accumulation within hours during incubation (Fig. S9). Nonetheless, elevated substrate concentrations did not exclusively enhance both NH_4^+ consumption pathways (Fig. 3), suggesting that the microbial community structure and interactions may also modulate particle-mediated responses of NH_4^+ consumption along the environmental gradient.

Along the estuarine continuum, ammonia-oxidizing populations shift from AOB dominance in freshwater to AOA prevalence seawards (Fig. S6), with contracting substrate affinities and kinetics (Martens-Habbena et al., 2009; Kits et al., 2017; Jung et al., 2022). In the AOB-dominant freshwater of the JRE, the half-saturation constant (K_m) for ammonia oxidation (30–40 μmol dm^{-3} at the ambient temperature of ~26 °C; Zheng et al., 2020) is comparable to the ambient NH_4^+ concentration at JRE-8 (34.5 μmol dm^{-3}; Fig. 2). Thus, in situ SPM addition likely stimulated AOR at substrate unsaturated conditions. This is supported by substrate kinetics experiments, which show enhanced AOR at elevated NH_4^+ concentrations in freshwater from the JRE at different temperatures (Zheng et al., 2020). Added SPM may also promote AOB growth and activity (Xia et al., 2009; Ma et al., 2021), as supported by field observations during a storm-driven SPM enrichment in the JRE, where bacterial *amoA* gene abundance in the freshwater increased approximately fourfold in a few days (Lin et al., 2023). By contrast, in the AOA-dominant high-salinity waters, K_m values for ammonia oxidation are extremely low (40–50 nmol dm^{-3} at similar temperature; Zheng et al., 2020), orders of magnitude lower than those in the AOB-dominant freshwater and ambient NH_4^+ concentrations (10–20 μmol dm^{-3}). Under such saturating conditions, in situ SPM addition and the resultant elevated NH_4^+ concentrations did not substantially enhance AOR in these waters, as we observed in the experiments (Fig. 3a).

The negligible response of AUR to in situ SPM addition in the freshwater and brackish water (Fig. 3b) suggests that the phytoplankton might be growing under saturating substrate concentrations, accompanied by competition with AOB. Culture and field studies have demonstrated that the K_m values for ammonium uptake by different phytoplankton groups span from 0.1 to 10 μmol dm^{-3}, depending on ambient conditions such as substrate concentrations and light intensity (Fan et al., 2003; Xu et al., 2019; Papacek et al., 2024, and references therein). Overall, the K_m values tend to be elevated in environments such as the JRE, where substrate concentrations are enriched and light availability is limited. However, these reported K_m values are considerably lower than the ambient NH_4^+ concentrations (exceeding 20 μmol dm^{-3}; Fig. 2). Moreover, NH_4^+ accumulation during the incubations in the control groups (i.e., in the absence of SPM addition) was more evident at the low-salinity station (Fig. S9), which may also support our inference. Furthermore, the markedly elevated NH_4^+ in the incubation system may suppress its uptake. The high-NH_4^+ induced inhibition of phytoplankton growth has been extensively reported in coastal waters (e.g., Glibert et al., 2016, and references therein). In contrast, positive AUR responses were observed in the high-salinity waters (Fig. 3b). This suggests that, when NH_4^+ concentrations decreased to ~10 μmol dm^{-3}, the substrate availability for the phytoplankton in these waters became presumably unsaturated and the phytoplankton greatly outcompeted AOA for substrate (Fig. S5).

Interestingly, although AOR and AUR were comparable between the saline water (JRE-3) and the seawater (JRE-1) at similar substrate levels, in situ SPM addition significantly enhanced both rates only in the seawater (Fig. 3). Given the distinct C/N ratios and $\delta^{13}C_{org}$ signatures of SPM collected from two sites, we propose that SPM origins (terrestrial vs. marine) are very likely to exert an additional control on the observed divergent responses of NH_4^+ consumption rates along the estuary.

3.4. Responses of seawater NH_4^+ consumption to riverine SPM addition

To further examine how SPM with different characteristics affects NH_4^+ consumption rates in the estuary, we performed riverine SPM addition experiments at the seawater end (JRE-1; also see Methods for details). Riverine SPM collected from the freshwater end (JRE-8) was predominantly terrestrial in origin, exhibiting a higher C/N ratio and a more depleted $\delta^{13}C_{org}$ value, compared to in situ SPM collected from the seawater end which was primarily marine-derived (Fig. 2). Analogous to the in situ SPM addition experiments (Fig. 3), adding riverine SPM to the seawater induced substantial increases in both AOR and AUR (Fig. 4a). Specifically, AOR experienced a 118 % increase (from 1.0 ± 0.1 to 2.2 ± 0.4 nmol N dm^{-3} h^{-1}), while AUR showed a 90 % increase (from 38.2 ± 5.0 to 72.6 ± 10.1 nmol N dm^{-3} h^{-1}). These enhancements were larger than those induced by in situ SPM amendments (Figs. 3 and 4a), likely due to the higher PN concentrations used in the riverine SPM treatments compared with the in situ SPM addition experiments (3.23 ± 0.05 μmol dm^{-3} vs. 2.54 ± 0.02 μmol dm^{-3}; Fig. S2). To account for this difference, we normalized the responses to equivalent PN increases (i.e., ~7 % above ambient; Fig. S1). Under this correction, AOR enhancement by riverine SPM addition (22.3 ± 4.6 %) was comparable to that induced by the equivalent addition of in situ SPM (15.9 ± 6.1 %), whereas AUR exhibited a different response, with riverine SPM inducing only a 17.3 ± 0.4 % increase, significantly lower than the 69.9 ± 5.8 % enhancement observed with in situ SPM (Fig. 4b).

These results demonstrate that marine-derived SPM exerts a stronger influence on NH_4^+ consumption than riverine SPM in the outer estuary, particularly for AUR. Fresh marine SPM, derived primarily from bacterioplankton, phytoplankton, and their detritus, is more bioavailable than the riverine/terrestrial SPM (Behnke et al., 2023). As a result, the labile SPM can more efficiently supply substrates for ammonium-assimilating microorganisms, and strongly stimulate AUR at the seawater end, where the substrate for phytoplankton remains unsaturated. This finding thus provides a compelling explanation for the different responses of AUR observed between the saline water and the seawater in the in situ SPM addition experiments (Fig. 3b).

4. Conclusion and implications

This study provides the first comprehensive assessment of how increasing SPM concentrations influence NH_4^+ consumption dynamics and the underlying mechanisms along the salinity gradient of a eutrophic estuary (Fig. 5). Overall, the addition of in situ SPM differentially stimulated AOR and AUR, with contrasting responses in the inner and outer estuaries. In substrate-replete freshwater, the SPM added substantially enhanced AOR by supplying additional substrates and creating favorable habitats for AOB, characterized by relatively high K_m values and a tendency to adhere to particles. However, the lack of significant responses of AUR reflected the sufficient substrate for the growth of bacterioplankton and phytoplankton. Conversely, adding in situ SPM led to a remarkable increase in AUR in seawater with diminished substrate availability. However, when riverine SPM was introduced, the increase

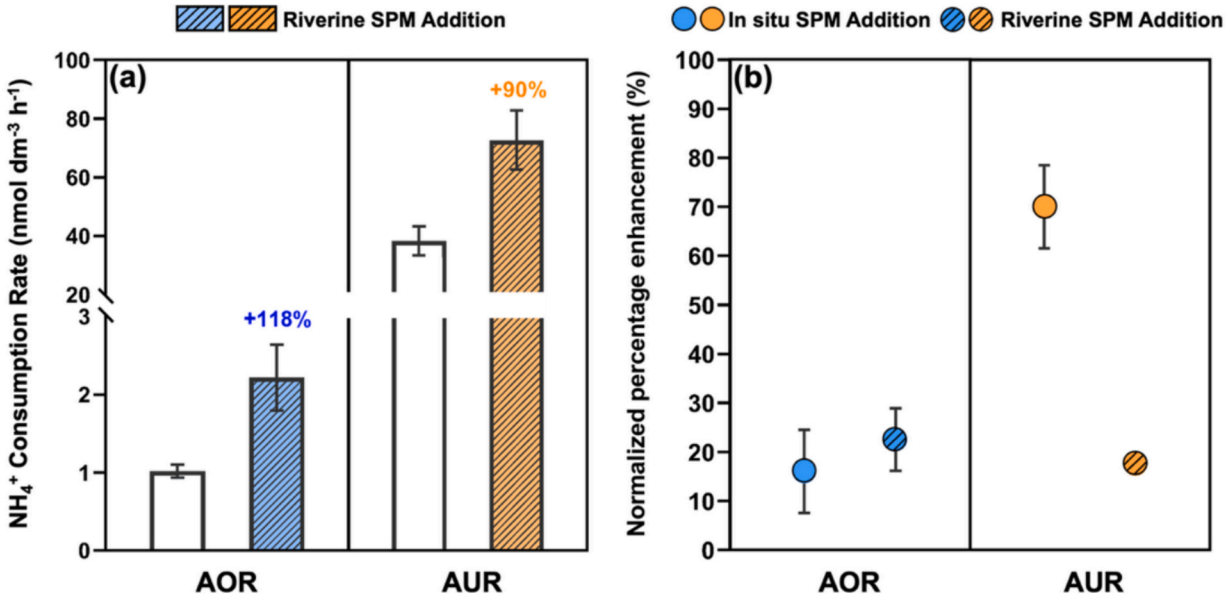

Fig. 4. (a) Responses of ammonia oxidation rates (AOR) and ammonium uptake rates (AUR) to riverine SPM addition at the seawater end (JRE-1). Hollow bars indicate the in situ rates without the addition of riverine SPM. Blue and orange slashed bars denote the rates by adding riverine SPM. Numbers indicate the increasing percentages relative to in situ rates. (b) Comparison of AOR and AUR percentage enhancements by adding in situ and riverine SPM at the seawater end. Note that, for comparison, the results for riverine SPM addition experiments have been normalized to equivalent in situ SPM added (Fig. S2). Solid color and forward-slash dots denote the enhancing effects of adding in situ and riverine SPM. (For interpretation of the references to color in this figure legend, the reader is referred to the web version of this article.)

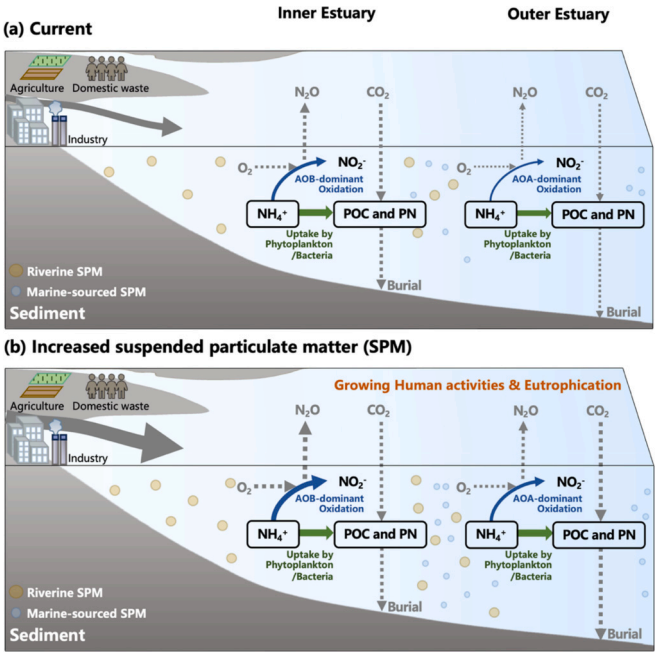

Fig. 5. Schematic diagram of particle-mediated NH_4^+ consumption pathways along the salinity gradient of the eutrophic and turbid estuary under current (a) and increasing SPM and nutrient export conditions (b). The brown and blue circles denote riverine and marine-sourced particles, respectively. The difference in arrow width indicates changes in rates of NH_4^+ consumption pathways in the inner and outer estuaries. (For interpretation of the references to color in this figure legend, the reader is referred to the web version of this article.)

in AUR was less pronounced. These results indicate that freshly produced marine SPM added can release NH_4^+ more efficiently to nourish phytoplankton and stimulate AUR, thereby outcompeting ammonia-oxidizing communities dominated by AOA in seawater.

Taken together, our study underscores that, under intensified anthropogenic activities and human-induced climate change, increasing SPM inputs have the potential to accelerate estuarine NH_4^+ dynamics and ultimately alter the associated biogeochemical processes (Fig. 5). Enhanced ammonia oxidation in the inner estuary may intensify N_2O emissions and DO consumption; on the other hand, elevated ammonium uptake in offshore regions could boost primary production and potentially contribute to marine carbon sequestration. Although riverine SPM is generally less bioavailable than marine SPM, its growing export to the ocean is likely to substantially stimulate NH_4^+ consumption in coastal ecosystems, with far-reaching implications for N cycling and ecosystem functioning.

CRediT authorship contribution statement

Sijing Kang: Writing – original draft, Visualization, Validation, Methodology, Investigation, Formal analysis, Data curation. **Shuran Yang:** Methodology, Investigation. **Min Nina Xu:** Writing – review & editing, Methodology. **Weiqiang Zhao:** Methodology, Investigation. **Jin-Ming Tang:** Writing – review & editing, Methodology. **Hongyan Bao:** Writing – review & editing, Resources. **Xiuli Yan:** Writing – original draft, Methodology. **Xiaolin Li:** Supervision, Resources. **Shuh-Ji Kao:** Writing – review & editing, Supervision, Resources, Conceptualization. **Jin-Yu Terence Yang:** Writing – review & editing, Writing – original draft, Supervision, Project administration, Funding acquisition, Conceptualization.

Declaration of competing interest

The authors declare that they have no known competing financial interests or personal relationships that could have appeared to influence the work reported in this paper.

Acknowledgments

We gratefully thank the Chief Editor, Michel C. Boufadel, and the anonymous reviewers for their constructive comments and suggestions,

which greatly improved the manuscript. This study is supported by the National Key Research and Development Program of China (No. 2022YFC3105304), the Natural Science Foundation of Xiamen, China (No. 3502Z202373015), the National Natural Science Foundation of China (No. 42476032, 42330401), and the Research Grants Council of the Hong Kong Special Administrative Region, China (No. AoE/P-601/23-N). We sincerely thank all crew members of RV *Ocean II* for their assistance. We thank Li Tian, Wenbin Zou, Yutong Yang, Lifang Wang, and Tao Huang for their help in sampling and sample measurements. We also thank Senwei Tong, Siqi Wu, and Moge Du for their valuable comments on data analysis and writing. We are grateful to the Center for Major Equipment and Technology (COMET) at the State Key Laboratory of Marine Environmental Science, Xiamen University, for its support of the instrumentation.

Appendix A. Supplementary data

Supplementary data to this article can be found online at https://doi.org/10.1016/j.marpolbul.2025.119027.

Data availability

The data for this manuscript are accessible in the Zenodo repository (https://doi.org/10.5281/zenodo.17240582).

References

Armstrong, F.A.J., Stearns, C.R., Strickland, J.D.H., 1967. The measurement of upwelling and subsequent biological process by means of the Technicon Autoanalyzer® and associated equipment. Deep-Sea Res. 14, 381–389.

Bartl, I., Hellemann, D., Rabouille, C., Schulz, K., Tallberg, P., Hietanen, S., Voss, M., 2019. Particulate organic matter controls benthic microbial N retention and N removal in contrasting estuaries of the Baltic Sea. Biogeosciences 16, 3543–3564.

Becker, S., Aoyama, M., Woodward, E.M.S., Bakker, K., Coverly, S., Mahaffey, C., Tanhua, T., 2020. GO-SHIP repeat hydrography nutrient manual: the precise and accurate determination of dissolved inorganic nutrients in seawater, using continuous flow analysis methods. Front. Mar. Sci. 7, 581790.

Behnke, M.I., Tank, S.E., McClelland, J.W., Holmes, R.M., Haghipour, N., Eglinton, T.I., Raymond, P.A., Suslova, A., Zhulidov, A.V., Gurtovaya, T., Zimov, N., Zimov, S., Mutter, E.A., Amos, E., Spencer, R.G.M., 2023. Aquatic biomass is a major source to particulate organic matter export in large Arctic rivers. Proc. Natl. Acad. Sci. USA 120 (12), e2209883120.

Berounsky, V.M., Nixon, S.W., 1993. Rates of nitrification along an estuarine gradient in Narragansett Bay. Estuaries 16, 718–730.

Bianchi, T.S., Mayer, L.M., Amaral, J.H.F., Arndt, S., Galy, V., Kemp, D.B., Kuehl, S.A., Murray, N.J., Regnier, P., 2024. Anthropogenic impacts on mud and organic carbon cycling. Nat. Geosci. 17 (4), 287–297.

Bowen, J.L., Giblin, A.E., Murphy, A.E., Bulseco, A.N., Deegan, L.A., Johnson, D.S., Nelson, J.A., Mozdzer, T.J., Sullivan, H.L., 2020. Not all nitrogen is created equal: differential effects of nitrate and ammonium enrichment in coastal wetlands. BioScience 70, 1108–1119.

Buchanan, P.J., Pierella Karlusich, J.J., Tuerena, R.E., Shafiee, R., Woodward, E.M.S., Bowler, C., Tagliabue, A., 2025. Relative enrichment of ammonium and its impacts on open-ocean phytoplankton community composition under a high-emissions scenario. Biogeosciences 22, 4865–4883.

Cai, X., Yao, L., Hu, Y., Jiang, H., Shen, M., Hu, Q., Wang, Z., Dahlgren, R.A., 2019. Particle-attached microorganism oxidation of ammonia in a hypereutrophic urban river. J. Basic Microbiol. 59, 511–524.

Casciotti, K.L., Sigman, D.M., Hastings, M.G., Böhlke, J.K., Hilkert, A., 2002. Measurement of the oxygen isotopic composition of nitrate in seawater and freshwater using the denitrifier method. Anal. Chem. 74, 4905–4912.

Dai, X., Chen, M., Wan, X., Tan, E., Zeng, J., Chen, N., Kao, S.J., Zhang, Y., 2022. Potential contributions of nitrifiers and denitrifiers to nitrous oxide sources and sinks in China's estuarine and coastal areas. Biogeosciences 19, 3757–3773.

Dai, M., Zhao, Y., Chai, F., Chen, M., Chen, N., Chen, Y., Cheng, D., Gan, J., Guan, D., Hong, Y., Huang, J., Lee, Y., Leung, K.M.Y., Lim, P.E., Lin, S., Lin, X., Liu, X., Liu, Z., Luo, Y.-W., Meng, F., Sangmanee, C., Shen, Y., Uthaipan, K., Wan Talaat, W.I.A., Wan, X.S., Wang, C., Wang, D., Wang, G., Wang, S., Wang, Y., Wang, Y., Wang, Z., Wang, Z., Xu, Y., Yang, J.-Y.T., Yang, Y., Yasuhara, M., Yu, D., Yu, J., Yu, L., Zhang, Z., Zhang, Z., 2023. Persistent eutrophication and hypoxia in the coastal ocean. Camb. Prism. Coast. Futures 1 (e19), 1–28.

Dugdale, R.C., Wilkerson, F.P., 1986. The use of ^{15}N to measure nitrogen uptake in eutrophic oceans; experimental considerations. Limnol. Oceanogr. 31 (4), 673–689.

Fan, C., Glibert, P.M., Burkholder, J.M., 2003. Characterization of the affinity for nitrogen, uptake kinetics, and environmental relationships for *Prorocentrum minimum* in natural blooms and laboratory cultures. Harmful Algae 2 (4), 283–299.

Galloway, J.N., Bleeker, A., Erisman, J.W., 2021. The human creation and use of reactive nitrogen: a global and regional perspective. Annu. Rev. Environ. Resour. 46 (1), 255–288.

Gardolinski, P.C.F.C., Hanrahan, G., Achterberg, E.P., Gledhill, M., Tappin, A.D., House, W.A., Worsfold, P.J., 2001. Comparison of sample storage protocols for the determination of nutrients in natural waters. Water Res. 35, 3670–3678.

Glibert, P.M., Wilkerson, F.P., Dugdale, R.C., Raven, J.A., Dupont, C.L., Leavitt, P.R., Parker, A.E., Burkholder, J.M., Kana, T.M., 2016. Pluses and minuses of ammonium and nitrate uptake and assimilation by phytoplankton and implications for productivity and community composition, with emphasis on nitrogen-enriched conditions. Limnol. Oceanogr. 61 (1), 165–197.

Gruber, N., Galloway, J., 2008. An Earth-system perspective of the global nitrogen cycle. Nature 451, 293–296.

Han, L.L., Wang, H., Ge, L., Xu, M.N., Tang, J.M., Luo, L., Li, P., Kao, S.J., 2023. Transition of source/sink processes and fate of ammonium in groundwater along with redox gradients. Water Res. 231, 119600.

Han, F., Tian, Q., Chen, N., Hu, Z., Wang, Y., Xiong, R., Xu, P., Liu, W., Stehr, A., Barra, R. O., Zheng, Y., 2024. Assessing ammonium pollution and mitigation measures through a modified watershed non-point source model. Water Res. 254, 121372.

Hou, X.J., Xie, D.H., Feng, L., Shen, F., Nienhuis, J.H., 2024. Sustained increase in suspended sediments near global river deltas over the past two decades. Nat. Commun. 15 (1), 3319.

Hsiao, S.S.Y., Hsu, T.C., Liu, J.W., Xie, X., Zhang, Y., Lin, J., Wang, H., Yang, J.Y.T., Hsu, S.C., Dai, M., Kao, S.J., 2014. Nitrification and its oxygen consumption along the turbid Chang Jiang River plume. Biogeosciences 11 (7), 2083–2098.

Jung, M.Y., Sedlacek, C.J., Kits, K.D., Mueller, A.J., Rhee, S.K., Hink, L., Nicol, G.W., Bayer, B., Lehtovirta-Morley, L., Wright, C., de La Torre, J.R., Herbold, C.W., Pjevac, P., Daims, H., Wagner, M., 2022. Ammonia-oxidizing archaea possess a wide range of cellular ammonia affinities. ISME J. 16, 272–283.

Kache, S., Bartl, I., Wäge-Recchioni, J., Voss, M., 2021. Influence of organic particle addition on nitrification rates and ammonium oxidiser abundances in Baltic seawater. Mar. Ecol. Prog. Ser. 674, 59–72.

Kennish, M.J., 2025. Eutrophication of estuarine and coastal marine environments: an emerging climatic-driven paradigm shift. Open J. Ecol. 15 (4), 289–324.

Kits, K.D., Sedlacek, C.J., Lebedeva, E.V., Han, P., Bulaev, A., Pjevac, P., Daebeler, A., Romano, S., Albertsen, M., Stein, L.Y., Daims, H., Wager, M., 2017. Kinetic analysis of a complete nitrifier reveals an oligotrophic lifestyle. Nature 549, 269–272.

Kitzinger, K., Padilla, C.C., Marchant, H.K., Hach, P.F., Herbold, C.W., Kidane, A.T., Könneke, M., Littman, S., Mooshammer, M., Niggemann, J., Petrov, S., Richter, A., Stewart, F.J., Wagner, M., Kuypers, M.M.M., Bristow, L.A., 2019. Cyanate and urea are substrates for nitrification by Thaumarchaeota in the marine environment. Nat. Microbiol. 4 (2), 234–243.

Kuypers, M., Marchant, H., Kartal, B., 2018. The microbial nitrogen-cycling network. Nat. Rev. Microbiol. 16, 263–276.

Lamb, A., Wilson, G., Leng, M., 2005. A review of coastal palaeoclimate and relative sea-level reconstructions using $\delta^{13}C$ and C/N ratios in organic material. Earth Sci. Rev. 75 (1–4), 29–57.

Laperriere, S.M., Nidzieko, N.J., Fox, R.J., Fisher, A.W., Santoro, A.E., 2019. Observations of variable ammonia oxidation and nitrous oxide flux in a eutrophic estuary. Estuar. Coasts 42 (1), 33–44.

Lee, Z., Shang, S., Qi, L., Yan, J., Lin, G., 2016. A semi-analytical scheme to estimate Secchi-disk depth from Landsat-8 measurements. Remote Sens. Environ. 177, 101–106.

Lee, Z., Shang, S., Lin, G., Liu, T., Liu, Y., Du, K., Luis, K., 2017. Secchi disk observation with spectral-selective glasses in blue and green waters. Opt. Express 25, 19878–19885.

Lin, J., Chen, N., Yuan, X., Tian, Q., Hu, A., Zheng, Y., 2020. Impacts of human disturbance on the biogeochemical nitrogen cycle in a subtropical river system revealed by nitrifier and denitrifier genes. Sci. Total Environ. 746, 141139.

Lin, J.J., Hu, A.Y., Wang, F.F., Hong, Y.G., Krom, M.D., Chen, N.W., 2023. Impacts of a subtropical storm on nitrogen functional microbes and associated cycling processes in a river-estuary continuum. Sci. Total Environ. 861, 160698.

Liu, X., Stock, C.A., Dunne, J.P., Lee, M.J., Shevliakova, E., Malyshev, S., Milly, P.C.D., 2021. Simulated global coastal ecosystem responses to a half-century increase in river nitrogen loads. Geophys. Res. Lett. 48 (17).

Liu, M., Raymond, P.A., Lauerwald, R., Zhang, Q., Trapp-Müller, G., Davis, K.L., Moosdorf, N., Xiao, C., Middelburg, J.J., Bouwman, A.F., Beusen, A.H.W., Peng, C., Lacroix, F., Tian, H., Wang, J., Li, M., Zhu, Q., Cohen, S., van Hoek, W.J., Li, Y., Li, Y., Yao, Y., Regnier, P., 2024. Global riverine land-to-ocean carbon export constrained by observations and multi-model assessment. Nat. Geosci. 17 (9), 896–904.

Liu, Y., Feng, Y., Han, S., Gao, Y., Xu, Z., 2025. Hotspots and future trends of estuarine nitrogen cycle: a bibliometric review. J. Hydrol. 657, 133056.

Ma, L., Tan, S., Liu, H., Kao, S.J., Dai, M., Yang, J.Y.T., 2021. Distribution and activity of ammonia-oxidizers on the size-fractionated particles in the Pearl River estuary. Front. Mar. Sci. 8, 685955.

Martens-Habbena, W., Berube, P.M., Urakawa, H., de La Torre, J.R., Stahl, D.A., 2009. Ammonia oxidation kinetics determine niche separation of nitrifying archaea and bacteria. Nature 461, 976–979.

Merbt, S.N., Stahl, D.A., Casamayor, E.O., Martí, E., Nicol, G.W., Prosser, J.I., 2012. Differential photoinhibition of bacterial and archaeal ammonia oxidation. FEMS Microbiol. Ecol. 327 (1), 41–46.

Middelburg, J.J., Nieuwenhuize, J., 2000. Uptake of dissolved inorganic nitrogen in turbid, tidal estuaries. Mar. Ecol. Prog. Ser. 192, 79–88.

Ormaza-González, F.I., Campi-Alvarez, P.A., Cárdenas-Condoy, J.W., Caiza-Quinga, R.J., Statham, P.J., 2024. Further evidence for increasing global near-shore

eutrophication from the Estero Salado, Guayaquil, Ecuador. Cont. Shelf Res. 278, 105271.
Papacek, J.R., Inglett, P.W., Phlips, E.J., Lasi, M.A., 2024. Nitrogen and phosphorus uptake kinetics in cultures of two novel picoplankton groups responsible for a recent bloom event in a subtropical estuary (Indian River Lagoon, Florida). Front. Mar. Sci. 11, 1256901.
Scanes, E., Scanes, P.R., Ross, P.M., 2020. Climate change rapidly warms and acidifies Australian estuaries. Nat. Commun. 11, 1803.
Sharples, J., Middelburg, J.J., Fennel, K., Jickells, T.D., 2017. What proportion of riverine nutrients reaches the open ocean? Glob. Biogeochem. Cycles 31, 39–58.
Sigman, D.M., Casciotti, K.L., Andreani, M., Barford, C., Galanter, M., Böhlke, J.K., 2001. A bacterial method for the nitrogen isotopic analysis of nitrate in seawater and freshwater. Anal. Chem. 73 (17), 4145–4153.
Stahl, D.A., de la Torre, J.R., 2012. Physiology and diversity of ammonia-oxidizing archaea. Ann. Rev. Microbiol. 66, 83–101.
Stein, L.Y., Yung, Y.L., 2003. Production, isotopic composition, and atmospheric fate of biologically produced nitrous oxide. Annu. Rev. Earth Planet. Sci. 31 (1), 329–356.
Strickland, J.D.H., Parsons, T.R., 1972. A Practical Handbook of Seawater Analysis, 2nd edition. Fisheries Research Board of Canada, Ottawa, Canada. https://doi.org/10.25607/OBP-1791. 310 pp. (Bulletin Fisheries Research Board of Canada, Nr. 167 (2nd ed)).
Tan, E., Zou, W., Zheng, Z., Yan, X., Du, M., Hsu, T.C., Tian, L., Middelburg, J.J., Trull, T. W., Kao, S.J., 2020. Warming stimulates sediment denitrification at the expense of anaerobic ammonium oxidation. Nat. Clim. Chang. 10 (4), 349–355.
Tanaka, Y., Minggat, E., Roseli, W., 2021. The impact of tropical land-use change on downstream riverine and estuarine water properties and biogeochemical cycles: a review. Ecol. Process. 10, 40.
Tang, J.M., Xu, M.N., Lin, Y.X., Chen, H.X., Jin, H.Q., Han, L.L., Zou, W., Kao, S.J., 2022. The biological transformation of ammonium and urea in a eutrophic estuarine system in Southern China. Front. Mar. Sci. 9, 1040554.
Tang, W., Fortin, S.G., Intrator, N., Lee, J.A., Kunes, M.A., Jayakumar, A., Ward, B.B., 2025. Contrasting oxygen sensitivities of ammonia oxidation and nitrous oxide production in estuarine waters. Environ. Sci. Technol. https://doi.org/10.1021/acs.est.5c06142.
Verdugo, P., Alldredge, A.L., Azam, F., Kirchman, D.L., Passow, U., Santschi, P.H., 2004. The oceanic gel phase: a bridge in the DOM–POM continuum. Mar. Chem. 92 (1–4), 67–85.
Wan, X.S., Sheng, H.X., Liu, L., Shen, H., Tang, W., Zou, W., Xu, M.N., Zheng, Z., Tan, E., Chen, M., Zhang, Y., Ward, B.B., Kao, S.J., 2023. Particle-associated denitrification is the primary source of N_2O in oxic coastal waters. Nat. Commun. 14 (1), 8280.
Wang, G.Z., Wang, Z.Y., Zhai, W.D., Moore, W.S., Li, Q., Yan, X., Qi, D., Jiang, Y.W., 2015. Net subterranean estuarine export fluxes of dissolved inorganic C, N, P, Si, and total alkalinity into the Jiulong River estuary, China. Geochim. Cosmochim. Acta 149, 103–114.
Wang, C., Ding, Y., Guo, Z., Lin, H., Wu, J., 2022. Spatial–temporal distribution of total organic carbon and its transportation in the Jiulong River Estuary. Sci. Rep. 12 (1), 9395.
Wang, S.Y., Lan, B.R., Yu, L.B., Xiao, M.Y., Qin, Y., Jin, Y.C., Zhou, Y.T., Armanbek, G., Ma, J.C., Wang, M.T., Jetten, M.S.M., Tian, H.Q., Zhu, G.B., Zhu, Y.G., 2024. Ammonium-derived nitrous oxide is a global source in streams. Nat. Commun. 15, 4085.
Wawrik, B., Paul, J.H., Bronk, D.A., John, D., Gray, M., 2004. High rates of ammonium recycling drive phytoplankton productivity in the offshore Mississippi River plume. Aquat. Microb. Ecol. 35 (2), 175–184.
Wu, G., Cao, W., Huang, Z., Kao, C.M., Chang, C.T., Chiang, P.C., Wang, F.F., 2017. Decadal changes in nutrient fluxes and environmental effects in the Jiulong River Estuary. Mar. Pollut. Bull. 124 (2), 871–877.
Xia, X.H., Yang, Z.F., Zhang, X.Q., 2009. Effect of suspended-sediment concentration on nitrification in river water: importance of suspended sediment-water interface. Environ. Sci. Technol. 43, 3681–3687.
Xu, M.N., Li, X., Shi, D.L., Zhang, Y., Dai, M., Huang, T., Glibert, P.M., Kao, S.J., 2019. Coupled effect of substrate and light on assimilation and oxidation of regenerated nitrogen in the euphotic ocean. Limnol. Oceanogr. 64, 1270–1283.
Xu, M.N., Wu, Y.H., Zhang, X., Tang, J.M., Tan, E., Zheng, Z.Z., Du, M., Yan, X., Kao, S.J., 2022. Diel change in inorganic nitrogenous nutrient dynamics and associated oxygen stoichiometry along the Pearl River Estuary. Water Res. 22, 118954.
Yan, X.L., Zhai, W.D., Hong, H.S., Li, Y., Guo, W.D., Huang, X., 2012. Distribution, fluxes and decadal changes of nutrients in the Jiulong River Estuary, Southwest Taiwan Strait. Chin. Sci. Bull. 57 (18), 2307–2318.
Yan, X.L., Wan, X.S., Liu, L., Xu, M.N., Tan, E., Zheng, Z.Z., Zou, W., Tian, L., Li, D.W., Trull, T.W., Kao, S.J., 2019. Biogeochemical dynamics in a eutrophic tidal estuary revealed by isotopic compositions of multiple nitrogen species. J. Geophys. Res. Biogeosci. 124 (7), 1849–1864.
Yang, J.Y.T., Kao, S.J., Dai, M., Yan, X., Lin, H.L., 2017. Examining N cycling in the northern South China Sea from N isotopic signals in nitrate and particulate phases. J. Geophys. Res. Biogeosci. 122 (8), 2118–2136.
Yang, J.Y.T., Hsu, T.C., Tan, E., Lee, K., Krom, M.D., Kang, S., Dai, M., Hsiao, S.S.Y., Yan, X., Zou, W., Tian, L., Kao, S.J., 2022. Sedimentary processes dominate nitrous oxide production and emission in the hypoxic zone off the Changjiang River estuary. Sci. Total Environ. 827, 154042.
Ye, F., Guo, W., Shi, Z., Jia, G.D., Wei, G.J., 2017. Seasonal dynamics of particulate organic matter and its response to flooding in the Pearl River Estuary, China, revealed by stable isotope ($\delta^{13}C$ and $\delta^{15}N$) analyses. J. Geophys. Res. Oceans 122 (8), 6835–6856.
Yu, D., Chen, N., Krom, M.D., Lin, J.J., Cheng, P., Yu, F.L., Guo, W.D., Hong, H.S., Gao, X. J., 2019. Understanding how estuarine hydrology controls ammonium and other inorganic nitrogen concentrations and fluxes through the subtropical Jiulong River Estuary, SE China under baseflow and flood-affected conditions. Biogeochemistry 142, 443–466.
Zhang, M., Krom, M.D., Lin, J., Cheng, P., Chen, N., 2022. Effects of a storm on the transformation and export of phosphorus through a subtropical river-turbid estuary continuum revealed by continuous observation. J. Geophys. Res. Biogeosci. 127, e2022JG006786.
Zhao, W., Bao, H., Peng, L., Du, M., Li, K., Zhan, X., Li, S., Tian, L., Huang, D., Zou, W., Yang, J.-Y.T., Kao, S.-J., 2025. Transport of dissolved black carbon in three estuaries in China: roles of flood-ebb tides and submarine groundwater discharge. Glob. Biogeochem. Cycles 39, e2025GB008532.
Zheng, Z.Z., Wan, X.S., Xu, M.N., Hsiao, S.S.Y., Zhang, Y., Zheng, L.W., Wu, Y.H., Zou, W., Kao, S.J., 2017. Effects of temperature and particles on nitrification in a eutrophic coastal bay in southern China. J. Geophys. Res. Biogeosci. 122 (9), 2325–2337.
Zheng, Z.Z., Zheng, L.W., Xu, M.N., Tan, E., Hutchins, D.A., Deng, W.C., Zhang, Y., Shi, D.L., Dai, M., Kao, S.J., 2020. Substrate regulation leads to differential responses of microbial ammonia-oxidizing communities to ocean warming. Nat. Commun. 11 (1), 3511.